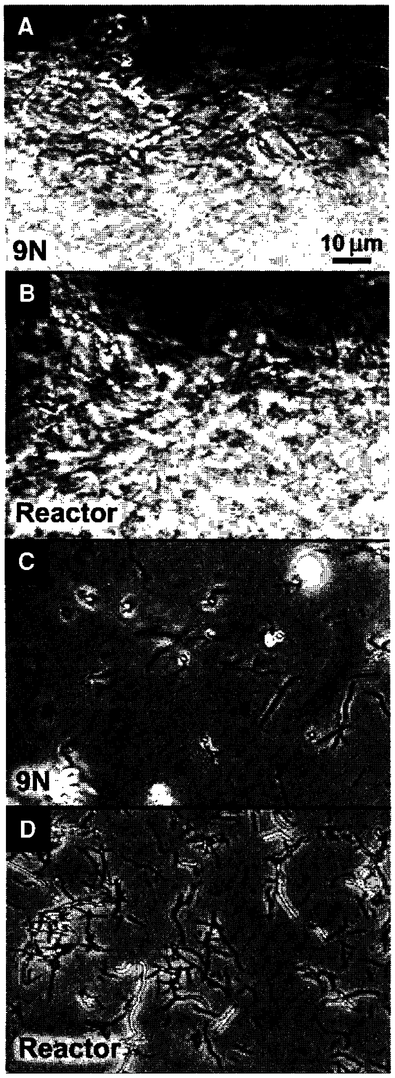

Fig. 5. Phase microscopic comparison of flocculent material from the 9°N snowblower vent and the laboratory reactor. (**A** and **B**) Intact flocs. (**C** and **D**) Filamentous material dispersed by vigorous physical mixing. Symbols: 9N, samples obtained from 9°N snowblower vent; Reactor, samples obtained from the laboratory reactor.

tangling, long, irregular filaments rather than as globular or amorphous sulfur, as found with most known sulfide oxidizers. By modification of the turbulent boundary layer, mats of these filaments may also be important in regulating the local microenvironment (for example, O_2-H_2S gradients) in which the organisms reside.

REFERENCES AND NOTES

1. J. M. Larkin and W. R. Strohl, *Annu. Rev. Microbiol.* **37**, 341 (1983).
2. H. W. Jannasch, C. O. Wirsen, S. J. Molyneaux, *Deep-Sea Res.* **38** (suppl. 2), S1105 (1991).
3. D. C. Nelson, C. O. Wirsen, H. W. Jannasch, *Appl. Environ. Microbiol.* **55**, 2909 (1989); H. W. Jannasch, in *Biology of Autotrophic Bacteria*, H. G. Schlegel and B. Bowien, Eds. (Science Technical, Madison, WI, 1989), pp. 147–166.
4. J. E. Hobbie, R. J. Daley, S. Jasper, *Appl. Environ. Microbiol.* **33**, 1225 (1977).
5. Filaments also completely dissolved under the microscope when seawater was gradually exchanged with ethanol, and they melted into spheres when illuminated by high-intensity near-ultraviolet (UV) light at the absorption band for sulfur (excitation bandpass, 340 to 390 nm). Both filaments and finely ground commercial sublimed elemental sulfur absorb sufficient near-UV radiation to be heated to their melting point, even when immersed in water. Filamentous sulfur washed in distilled water and steam sterilized (three times at 110°C) supported chemolithoautotrophic growth of two *Thiomicrospira* species (*16*). Both organisms grew nearly as quickly on the filamentous sulfur as they did on soluble thiosulfate, and twice as fast as when grown on commercial sublimed elemental sulfur. Ethanol solubility and ease of microbial utilization probably reflect the hydrophilic nature of the filaments.
6. R. Steudel, in *Biology of Autotrophic Bacteria*, H. G. Schlegel and B. Bowien, Eds. (Science Technical, Madison, WI, 1989), pp. 289–303; R. Steudel, G. Holdt, P. T. Visscher, H. van Gemerden, *Arch. Microbiol.* **153**, 432 (1990).
7. R. Steudel, T. Gobel, G. Holdt, *Z. Naturforsch. Teil B* **43**, 203 (1988); R. Steudel, G. Holdt, T. Gobel, *J. Chromatogr.* **475**, 442 (1989).
8. Sterile reactors and inoculated reactors poisoned with glutaraldehyde or sodium azide failed to produce filaments. Radioisotopic experiments using cleaned suspensions of the vibrio (>99.5% vibrios) showed that they were able to fix CO_2 maximally at sulfide concentrations between 500 and 1500 µM and continued fixing CO_2 at 2000 µM, a concentration that is toxic for previously described hydrothermal-vent sulfur oxidizers (*16*).
9. C. O. Wirsen and H. W. Jannasch, *J. Bacteriol.* **136**, 765 (1978); C. O. Wirsen, personal observations.
10. C. D. Taylor, personal observations.
11. R. M. Haymon *et al.*, *Earth Planet. Sci. Lett.* **119**, 85 (1993).
12. K. Rubin II, J. D. Macdougall, M. R. Perfit, *Nature* **368**, 841 (1994).
13. D. Nelson, R Haymon, M. Lilley, *Eos* **72**, 481 (1991).
14. This material was collected and provided by D. Nelson (Univ. of California, Davis).
15. Like the laboratory reactor filaments, the vent filamentous material was not stainable with acridine orange, was soluble in alcohol, and exhibited an identical melting response under the microscope when exposed to near-UV light.
16. E. G. Ruby and H. W. Jannasch, *J. Bacteriol.* **149**, 161 (1982); H. W. Jannasch, C. O. Wirsen, D. C. Nelson, L. A. Robertson, *Int. J. Syst. Bacteriol.* **35**, 422 (1985).
17. H. W. Jannasch and C. O. Wirsen, *Appl. Environ. Microbiol.* **41**, 525 (1981).

18. We thank S. J. Molyneaux, D. Wiebe, and L. Hare for assistance with technical aspects of this work. Woods Hole Oceanographic Institution contribution 9432. Supported by grant IBN96-30054 from NSF.

12 May 1997; accepted 14 July 1997

The Isotopic Oxygen Nightglow as Viewed from Mauna Kea

T. G. Slanger,* D. L. Huestis, D. E. Osterbrock, J. P. Fulbright

Optical spectra of the terrestrial nightglow in the 520- to 900-nanometer region, as measured by the W. M. Keck telescope on Mauna Kea in Hawaii and the associated high-resolution echelle spectrograph, showed many bands belonging to the important $O_2(b\text{-}X)$ Atmospheric Band emission system. Previous ground-based measurements have shown only a single band, from the lowest vibrational level of the emitting state. Of particular interest is the fact that at the 762-nanometer position of the *b-X* 0-0 band, where earlier studies have shown only absorption features, these results showed both absorption at the $^{16}O^{16}O$ line positions and well-resolved emission at the positions of many of the $^{18}O^{16}O$ and $^{17}O^{16}O$ lines. These findings show that substantial advances can be made in understanding atmospheric emission phenomena by the use of astronomical tools.

The terrestial nightglow is the emission in the upper atmosphere, typically in the 80- to 100-km altitude region, originating from chemical reactions and atom recombination processes. As seen from the ground, this emission is dominated by two emitting molecular species, O_2 and OH. The OH emission is in the ground-state Meinel band system, beginning near 520 nm and extending well into the infrared region (*1*). O_2 emission is found in the near ultraviolet from the Herzberg band systems (*2*) and in the red and infrared from the Atmospheric ($b^1\Sigma_g^+ - X^3\Sigma_g^-$) and Infrared Atmospheric ($a^1\Delta_g - X^3\Sigma_g^-$) Band systems (*3, 4*). The $a^1\Delta_g$ and $b^1\Sigma_g^+$ states of oxygen are the first and second electronically excited states, respectively (*5*). The region between 600 and 900 nm has typically been considered to be almost barren of molecular oxygen emission features, but we show here that with sufficient resolution and sensitivity, this region contains a great deal of spectral information, pertaining to atmospheric energy flow and the photochemistry of O_2, that can be extracted from ground-based observation.

As many astronomical measurements are made in the 600- to 900-nm region, considerable effort has been expended in accurately determining the positions of the ubiquitous

---

T. G. Slanger and D. L. Huestis, Molecular Physics Laboratory, SRI International, 333 Ravenswood Avenue, Menlo Park, CA 94025, USA.
D. E. Osterbrock and J. P. Fulbright, University of California Observatories/Lick Observatory, University of California, Santa Cruz, CA 95064, USA.

*To whom correspondence should be addressed. E-mail: slanger@mplvax.sri.com

OH lines, which are useful for spectral calibration of the radiation from astronomical objects. A study was recently completed for this purpose (*1*) that used the high spectral resolving power of the high-resolution echelle spectrograph (HIRES), which is coupled to the Keck telescope, and the sky spectra that are routinely obtained during astronomical observations. Although OH was the target for this investigation, the detector sensitivity and the optical resolution (0.02 nm) are high enough for detection of O_2 Atmospheric Bands from vibrationally excited levels. In the original publication (*1*), emission spectra from the vibrational quantum number $v = 3$ and 4 levels of the $O_2(b^1\Sigma_g^+)$ state were presented. In the many previous nightglow studies, only the lowest $v = 0$ level had been seen.

We have now carefully scrutinized the Keck spectra and found numerous interesting and important features. This paper emphasizes the isotopic lines observed in the 762-nm region, but there is much to be learned about the vibrational development in the $b^1\Sigma_g^+$ state and the so-called nightglow continuum. The latter can be quantified, because the O_2 absorption spectra observed in the present work define the depth of the continuum, which is the background emission against which the absorption is observed. The nightglow continuum is a glow of somewhat uncertain origin, which has components of atmospheric emissions (*6*) (for example, electronically excited NO_2), as well as radiation from stars and galaxies.

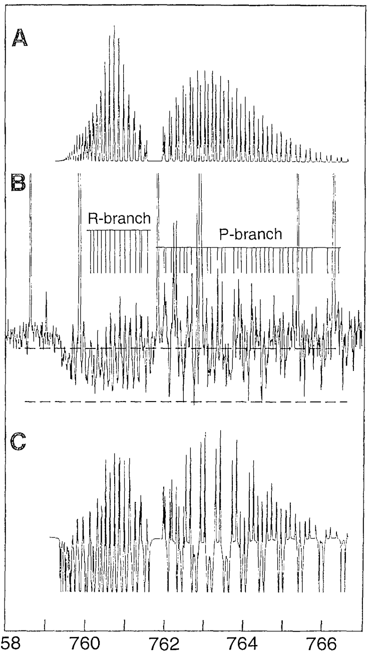

Fig. 1. (**A**) DIATOM spectral simulation of the $^{18}O^{16}O(b\text{-}X)$ 0-0 band in emission. The R-branch contains subbranches ^RR and ^RQ, whereas the P-branch has subbranches ^PP and ^PQ (*18*). (**B**) The HIRES spectrum in the region of the $O_2(b\text{-}X)$ 0-0 band. The positions of the $^{18}O^{16}O$ lines are marked. The two horizontal lines define the magnitude of the nightglow continuum, the portion that originates in the upper atmosphere and beyond. Off-scale lines are due to OH. (**C**) DIATOM $^{18}O^{16}O(b\text{-}X)$ 0-0 emission band simulation plus a continuum emission contribution, convolved with a DIATOM simulation of the $^{16}O^{16}O$ and $^{18}O^{16}O(b\text{-}X)$ 0-0 bands in absorption (text).

The atmosphere is largely transparent to the OH emission lines, but the same is not true for the O_2 *a-X* and *b-X* systems, at least for those transitions that terminate on $v = 0$ of the ground state. Typical nightglow intensities of the $O_2(b\text{-}X)$ 0-0 band (the transition between the $v = 0$ levels in both the upper and lower electronic states) are substantial when viewed from rockets or satellites, on the order of 5 kilorayleighs (kR) (*7*), but no discernible amount of this radiation has ever been reported to reach the ground, because of the very large line-of-sight O_2 optical depth from the emitting region.

The $O_2(b^1\Sigma_g^+)$ state in the nightglow is generated directly or indirectly from the recombination of oxygen atoms (*7, 8*) and is thus a marker for the O atom density in the 85- to 105-km region. In addition, the state is copiously produced in a secondary reaction when ozone is photodissociated by solar ultraviolet radiation in the stratosphere and is generated by solar resonance excitation in the *b-X* 0-0 band (*9*). Peak dayglow intensities of ~100 kR have been observed (*10*) and successfully simulated (*11*).

The $O_2(b\text{-}X)$ optical transition is strongly forbidden and has a radiative lifetime of 12 s, calculated from the absorption cross section (*12*). Upon absorption of the 0-0 band in the atmosphere by O_2, there is little chance of re-emission, because of quenching by N_2. For zenith observations, most absorption in the atmosphere takes place between 35 and 55 km, but the $b(v = 0)$ population can be measured from the ground, as the *b-X* 0-1 band at 864 nm can be detected (*1*) and it is not significantly absorbed in the atmosphere. The intensity ratio $I_{0\text{-}0}/I_{0\text{-}1}$ under optically thin conditions is 20 (*13*).

Babcock and Herzberg (*14*) measured absorption by O_2 against the solar continuum and showed that the $O_2(b\text{-}X)$ 0-0 lines are substantially broadened as a consequence of the large optical absorption depth. It appears that since these early measurements were made, little attention has been paid to that spectral region in terms of ground-based measurements. The opacity effect is well known and also affects emitters other than O_2. For instance, recent spectral measurements on "red sprites," the transient high-altitude emission associated with lightning strikes (*15*), have shown that the N_2 First Positive emission near 762 nm is greatly depleted (*16*). The O_2 absorption effect is accentuated by the 80° zenith angle at which the phenomenon is observed, so the O_2 optical depth is far greater than for vertical observations.

The experimental spectrum in the region of the $O_2(b\text{-}X)$ 0-0 band, taken with HIRES, is shown in Fig. 1B. It contains substantial structure, demonstrating that the region is not uniformly opaque. This has been clear since Babcock and Herzberg's measurements (*14*). They showed, in solar continuum absorption, that many of the lines of the $^{18}O^{16}O(b\text{-}X)$ 0-0 band are separated from the broadened lines of the normal isotope. Thus, it is reasonable to expect that, with sufficient resolution and sensitivity, the isotopic nightglow of O_2 should be discernible; the isotopic abundance percentages are 99.76, 0.037, and 0.204 for ^{16}O, ^{17}O, and ^{18}O, respectively.

In the calculated emission spectrum of the $^{18}O^{16}O(b\text{-}X)$ 0-0 band (Fig. 1A), made at 0.02-nm spectral resolution, with the DIATOM spectral simulation program (*17*), the intensity of the strongest R-branch lines is about 50% greater than that of the strongest P-branch lines, whereas the reverse is seen in the HIRES spectrum (Fig. 1B). This observation is a consequence of $^{16}O^{16}O$ absorption, as shown below. The comb-like structures in Fig. 1B show the lines appearing in the HIRES spectrum that clearly belong to the $^{18}O^{16}O$ isotopic band.

It is important to realize that the present observations are made possible by spectroscopic serendipity. Because $^{16}O^{16}O$ has identical nuclei, only alternate rotational levels exist. As this is not a restriction for the isotopic molecules, the $^{17}O^{16}O$ and $^{18}O^{16}O$ molecules have twice as many lines, and it is chiefly the alternate lines that have no match in $^{16}O^{16}O$ that are atmospherically transmitted. Because the HIRES spectrum is a combination of absorption and emission lines, we define a nightglow continuum intensity in Fig. 1B, where the minima in the absorption lines give the zero continuum level and the unattenuated continuum intensity derives from the adjoining spectral region.

To convert the calculated spectrum of Fig. 1A into an approximation of the HIRES spectrum, it is necessary to determine an absorption line profile for the $^{16}O^{16}O$ and $^{18}O^{16}O$ lines. Detailed treatments exist (*18*), although an extensive analysis is not warranted by the present data. The absorption lines near the point of origin of the emission have Gaussian line shapes, with a 200 K Doppler width of 0.02 cm^{-1}, but lower in the atmosphere, pressure broadening becomes important, and the line profile becomes intermediate between Gaussian and Lorentzian. A complication in the analysis is that observations obtained with the telescope pointed at various astronomical objects were not made at a constant O_2 column depth or for the present purpose. The data were taken at zenith angles between 25° and 50°. The secants of these angles, 1.10 and 1.55, average to 1.32, the factor by which the overhead column must be multiplied to obtain an average column depth. Thus, it would not be appropriate to use sophisticated procedures to analyze the spectrum.

At the 4.2-km elevation of Mauna Kea, the vertical O_2 column depth is 2.5×10^{24} cm^{-2}, leading to a value of 3.3×10^{24} cm^{-2} for the present observations. To calculate the absorption line profile, we used a Lorentzian absorption line shape with a linewidth of 0.05 cm^{-1} at a temperature of 240 K. The emission lines were given the Doppler linewidth of 0.02 cm^{-1} at a temperature of 200 K.

We obtained Fig. 1C by convolving the calculated 240 K $^{16}O^{16}O$ and $^{18}O^{16}O$ absorption spectra with the 200 K $^{18}O^{16}O$ emission spectrum of Fig. 1A and then adding a constant continuum level. The relative amplitudes of the line and continuum contributions were adjusted to approximately fit the experimental data. The final spectrum was then degraded to 0.34-cm^{-1} resolution to match the instrumental linewidth. It can be seen in Fig. 1C that the model reproduces the three major gaps in the P-branch and that the R-branch has become weaker than the P-branch. Thus, agreement is satisfactory in the important details. In comparing Figs. 1B and 1C, various extraneous lines may be seen in the former that do not appear to be associated with O_2 features. These extraneous lines are not surprising; there are OH lines throughout the spectral region, many of them not yet identified, and the data are currently being analyzed.

These spectroscopic observations are fascinating examples of simultaneous absorption and emission, made possible by three physical effects. First, the unattenuated 0-0 band intensity is large enough (~5 kR) for the small fraction arising from the minor isotopes to be detected. Second, the fact that there are twice as many $^{18}O^{16}O$ emission lines as $^{16}O^{16}O$ absorption lines results in spectral separation. Third, the low intensity of the continuum against which the absorption is viewed is comparable in magnitude to the emission signal. In contrast, it would be impossible to detect these emissions in either a solar or lunar absorption experiment.

The Keck data show another example of absorption, the b-X 1-0 band at 686 nm (Fig. 2). The work of Babcock and Herzberg (*14*) demonstrated that this transition is also optically thick. No emission is expected because the unattenuated 1-0 emission is weak, both because of rapid atmospheric quenching of the $v = 1$ level by O_2 (*19*) and the small Franck-Condon factor of the 1-0 band (*13*). Nevertheless, it is apparent that there are emission lines present in Fig. 2. These emission lines have not yet been identified but are presumably due to one of the many b-X emission bands appearing in the data.

As our calculations have been based on the heavier isotope, a remaining question is the relation between $^{18}O^{16}O$ and $^{17}O^{16}O$ line intensities. The absolute peak absorption cross section in the $^{16}O^{16}O$ 0-0 band for a 0.05-cm^{-1}-wide line is 1×10^{-22} cm^2 (*13*). When one uses an O_2 column depth of 3.3×10^{24} cm^{-2}, the optical depth (OD) at line center is 330. Calculating self-absorption by $^{18}O^{16}O$, we found an OD of $330(0.00204 \times 2) = 1.4$, leading to the conclusion that only 25% of nightglow emission from the strongest $^{18}O^{16}O$ lines reaches the ground for the conditions of these observations.

The amount of $^{17}O^{16}O$ in the atmosphere is smaller than that of $^{18}O^{16}O$ by a factor of 5.5. Thus, its OD is 0.25, and 78% of its radiation would reach the ground. On the assumption that the $O_2(b$-$X)$ 0-0 emission exhibits isotopic ratios in accord with natural abundances, the intensity ratio $I^{17}O^{16}O/I^{18}O^{16}O$ should be $0.78/(5.5 \times 0.25) = 0.57$, and 36% of the detected signal should be due to $^{17}O^{16}O$. This value is dependent on the actual OD (proportional to the secant of the zenith angle), and for the most strongly absorbed lines, a doubling of the OD will increase the percentage of $^{17}O^{16}O$ emission to 65%.

Pursuing this point will require data with still better spectral resolution, to separate the lines of the two heavier isotopes. In the R-branch, the few isolated $^{17}O^{16}O$ lines may suffer interference from b-X 8-7 band lines. In the P-branch, the lines of the two isotopes tend to be coincidental at 0.02-nm resolution, separating only at higher rotational levels where there are numerous extraneous lines.

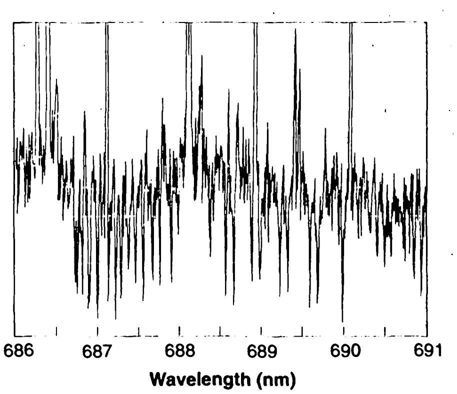

Fig. 2. HIRES spectrum in the region of the $O_2(b$-$X)$ 1-0 band, with the absorption lines superimposed on the nightglow continuum. Off-scale lines are due to OH.

Nevertheless, it is important to ascertain whether the nightglow emission intensities are in accord with the terrestrial isotopic ratios, and data taken with an experimental protocol specifically designed to investigate the O_2 nightglow would clarify this and other outstanding questions.

This study shows that there is much more spectral information available from ground-based observations than heretofore recognized. The critical parameter is optical resolution, and spectra taken at 0.02-nm resolution have enabled us to show that the 762-nm region is a rich source of isotopic information and also that it provides data on the nightglow continuum. It should be possible, in other regions, to demonstrate the presence of numerous $O_2(b$-$X)$ emission bands, from highly excited vibrational levels.

REFERENCES AND NOTES

1. D. E. Osterbrock *et al.*, *Publ. Astron. Soc. Pac.* **108**, 277 (1996).
2. A. L. Broadfoot and K. R. Kendall, *J. Geophys. Res.* **73**, 426 (1968).
3. R. J. Sica, *Can. J. Phys.* **69**, 1069 (1991).
4. R. Rodrigo, J. J. Lopez-Moreno, M. Lopez-Puertas, A. Molina, *J. Atmos. Terr. Phys.* **47**, 1099 (1985).
5. As elaborated in the classic spectroscopy text [G. Herzberg, *Molecular Spectra and Molecular Structure I. Spectra of Diatomic Molecules* (Van Nostrand Reinhold, New York, 1950)], electronic states of diatomic molecules are named and described by composite symbols of the form $X^3\Sigma_g^-$. X is the name of the state (the ground state); the superscript 3 indicates the electron spin degeneracy (triplet); Σ indicates the projection of electron orbital angular momentum (Σ and Δ mean 0 and 2); the subscript g indicates parity of the electronic wave function with respect to inversion through the center of mass (gerade or symmetrical); and for Σ states, the superscript $-$ indicates the parity of the electronic wave function with respect to reflection through a plane containing the nuclei ($-$ means antisymmetrical).
6. I. C. McDade, E. J. Llewellyn, R. G. H. Greer, D. P. Murtagh, *Planet. Space Sci.* **34**, 801 (1986).
7. I. C. McDade *et al.*, *Planet. Space Sci.* **34**, 780 (1986).
8. G. Brasseur and D. Offermann, *J. Geophys. Res.* **91**, 10818 (1986).
9. M. G. Mlynczak, *Geophys. Res. Lett.* **20**, 1439 (1993).
10. L. Wallace and D. M. Hunten, *J. Geophys. Res.* **73**, 4813 (1968).
11. A. Bucholtz, W. R. Skinner, V. J. Abreu, P. B. Hays, *Planet. Space Sci.* **34**, 1031 (1986).
12. D. E. Burch and D. A. Gryvnak, *Appl. Opt.* **8**, 1493 (1969).
13. P. H. Krupenie, *J. Phys. Chem. Ref. Data* **1**, 423 (1972).
14. H. D. Babcock and L. Herzberg, *Astrophys. J.* **108**, 167 (1948).
15. D. D. Sentman, E. M. Wescott, D. L. Osborne, D. L. Hampton, M. J. Heavner, *Geophys. Res. Lett.* **22**, 1205 (1995).
16. S. B. Mende, R. L. Rairden, G. R. Swenson, W. A. Lyons, *ibid.*, p. 2633.
17. D. L. Huestis, DIATOM Spectral Simulation Program, Version 7 (SRI International, Menlo Park, CA, 1994).
18. K. J. Ritter and T. D. Wilkerson, *J. Mol. Spectrosc.* **121**, 1 (1987).
19. L. C. Lee and T. G. Slanger, *J. Chem. Phys.* **69**, 4053 (1978).
20. We thank the Keck observers listed in (*1*), whose spectral data provided the basis for this paper, P. C. Cosby

for carrying out spectroscopic calculations on the oxygen transitions, and R. A. Copeland for his contributions. The W. M. Keck Observatory is operated by the California Institute of Technology and the University of California. D.E.O. and J.P.F. acknowledge NSF for partial support of this research under grant AST 91-23547. T.G.S. and D.L.H. acknowledge support by NASA Space Physics Division under grant NAGW-3669.

14 February 1997; accepted 17 July 1997

Detection of Soft X-rays and a Sensitive Search for Noble Gases in Comet Hale-Bopp (C/1995 O1)

Vladimir A. Krasnopolsky,* Michael J. Mumma, Mark Abbott, Brian C. Flynn, Karen J. Meech, Donald K. Yeomans, Paul D. Feldman, Cristiano B. Cosmovici

An image of comet Hale-Bopp (C/1995 O1) in soft x-rays reveals a central emission offset from the nucleus, as well as an extended emission feature that does not correlate with the dust jets seen at optical wavelengths. Neon was found to be depleted in the cometary ice by more than a factor of 25 relative to solar abundance, which suggests that ices in Hale-Bopp formed at (or later experienced) temperatures higher than 25 kelvin. A helium line emission at a wavelength of 584 angstroms was detected and may be attributable to charge transfer of solar wind α particles in the cometary coma. Ionized oxygen and another helium line contribute to an emission observed at 538 angstroms.

The Extreme Ultraviolet Explorer satellite (EUVE) provides spectroscopic measurements of celestial objects in a wavelength range of 70 to 760 Å and imaging in a 70 to 180 Å (≈ 180 to 70 eV) bandpass (*1*). At 760 Å, the photon energy (16.3 eV) exceeds the bond energies in molecules and the ionization potentials of most neutral atoms (except He, Ne, and F); hence, only spectral lines of He, Ne, F, and atomic ions are expected in the extreme ultraviolet (EUV) spectra of comets. He and Ne have resonance lines in this range, and abundances of Ne could serve to constrain the temperature at which precometary ices formed. Only upper limits to abundances of He, Ne, and Ar have been established in comets (*2*), but those for Ne and Ar exceeded the solar abundances by more than an order of magnitude. Solar light is faint in the EUV, so even the strongest EUV emissions from bodies such as the moon, Mars, and Jupiter are near the detection limit (*3*).

Hale-Bopp (C/1995 O1) is perhaps the biggest and brightest comet of this century; its nucleus mass may exceed that of comet 1P/Halley by a factor of 40 (*4*). Our EUVE observation of Hale-Bopp was acquired from 14 to 19 September 1996, when the comet was at heliocentric and geocentric distances $r = 3.07$ AU and $\Delta = 2.91$ AU, respectively. The total exposure time was 1.4×10^5 s, and its effective value was reduced to $\tau = 9 \times 10^4$ s as a result of filtering (*5*).

A soft x-ray image of Hale-Bopp in the range of 70 to 180 eV was obtained and corrected for background and for a known vignetting function (*6*). To improve the signal-to-noise ratio, we convolved the image with a Gaussian having a radius at half-maximum of 1.5×10^5 km (Fig. 1A). An optical image (Fig. 1B), enhanced to show dust jets more clearly (*7*), does not correlate with the x-ray image. The x-ray emission is not centered on the expected position of the nucleus. The center of brightness is offset relative to the expected position of the nucleus by 1.4 (±0.6) × 10^5 km in the sky plane. If the brightness center lies on the sun's azimuth, then the distance of the brightness center from the nucleus is 2.7 (±1.2) × 10^5 km (*8*). The center of brightness is between the radius vector to the sun and the comet velocity vector, and an extended region of emission is seen toward the southwest. A weak feature in the antivelocity direction is also seen.

The soft x-ray brightness varies with distance from the brightness center ρ_0 (Fig. 2). The x-ray brightness in Hale-Bopp is maximum at 0.005 rayleighs and decreases by a factor of 3 to $\rho_0 = 2 \times 10^5$ km. The production rate of x-ray photons Q_x is 8 (±2) × 10^{24} photons s^{-1} for $\rho_0 = 4 \times 10^5$ km (*9*, *10*) (Fig. 3). If charge transfer is a dominant excitation process, then [using a spectrum from (*10*) and our measurement] we expect a total x-ray ($E > 80$ eV) luminosity of 3.5×10^{25} and 2.6×10^{25} photons s^{-1} for $\rho = 4 \times 10^5$ and 2.5×10^5 km, respectively.

The Ne 736 Å line is traditionally used as a tool to search for Ne. However, the second resonance line for Ne (the analog of Lyman-β) at 630 Å coincides with a strong emission line in the solar spectrum and therefore provides better detection prospects than the 736 Å line, by two orders of magnitude (*12*). The advantage of the 630 Å line reaches three orders of magnitude for EUVE, which has a lower efficiency at 736 Å than at 630 Å.

No cometary signal is seen at 630 Å, and a 2σ upper limit corresponds to 45 counts for the largest bin (Fig. 4); this limit corresponds to $Q_{Ne} < 4 \times 10^{27}$ s^{-1} (*13*). The production rate of oxygen (as H_2O, CO, and CO_2) was equal to 6.6×10^{29} s^{-1} during the observation (*4*). Hence, the Ne/O ratio in the gas alone is $<6 \times 10^{-3}$ in Hale-Bopp. The ratio of oxygen in the dust and gas was 1.3 in comet 1P/Halley (*14*). Scaling to the dust and gas productions in both comets (*4*, *15*), we find that this ratio is ~8 in Hale-

Table 1. Observations of soft x-rays in Hyakutake and Hale-Bopp. X-ray data for Hyakutake are from (*37*); *r* is the heliocentric distance, Q_x is the x-ray photon production rate observed within a cometocentric radius ρ_0, ρ_B is the offset of the brightness center from the nucleus, Q_{gas} is the gas production rate (*4*, *38*), and $Af\rho$ is proportional to the dust production rate (*4*, *38*). $Af\rho_x$ is discussed in (*35*).

Parameter	Hyakutake	Hale-Bopp
r (AU)	1.07	3.07
Q_x (photons s^{-1})	1 (±0.2) × 10^{25}*	8 (±2) × 10^{24}
ρ_0 (km)	1.2 × 10^5	4 × 10^5
ρ_B (km)	5.6 (±1) × 10^4†	2.7 (±1.2) × 10^5
Q_{gas} (s^{-1})	2 × 10^{29}	6 × 10^{29}
$Af\rho$ (m)	79	630
$(Af\rho)_x$ (m)	3700	7500
$(Af\rho)_x/Af\rho$	47	12

*10^{25} photons s^{-1} from (*34*). †3 x 10^4 km from (*34*).

V. A. Krasnopolsky, Catholic University of America, Washington, DC 20064, USA, and NASA Goddard Space Flight Center, Greenbelt, MD 20771, USA.
M. J. Mumma, NASA Goddard Space Flight Center, Greenbelt, MD 20771, USA.
M. Abbott and B. C. Flynn, Center for Extreme Ultraviolet Astrophysics, Berkeley, CA 94720, USA.
K. J. Meech, Institute for Astronomy, Honolulu, HI 96822, USA.
D. K. Yeomans, Jet Propulsion Laboratory, Pasadena, CA 91109, USA.
P. D. Feldman, Johns Hopkins University, Baltimore, MD 21218, USA.
C. B. Cosmovici, Istituto Fisica Spazio Interplanetario, CNR, 00044 Frascati, Italy.

*To whom correspondence should be addressed (at NASA). E-mail: ys2VK@lepvax.gsfc.nasa.gov